Volume 58
Number 65
21 August 2022
Pages 9041–9162

ChemComm

Chemical Communications

rsc.li/chemcomm

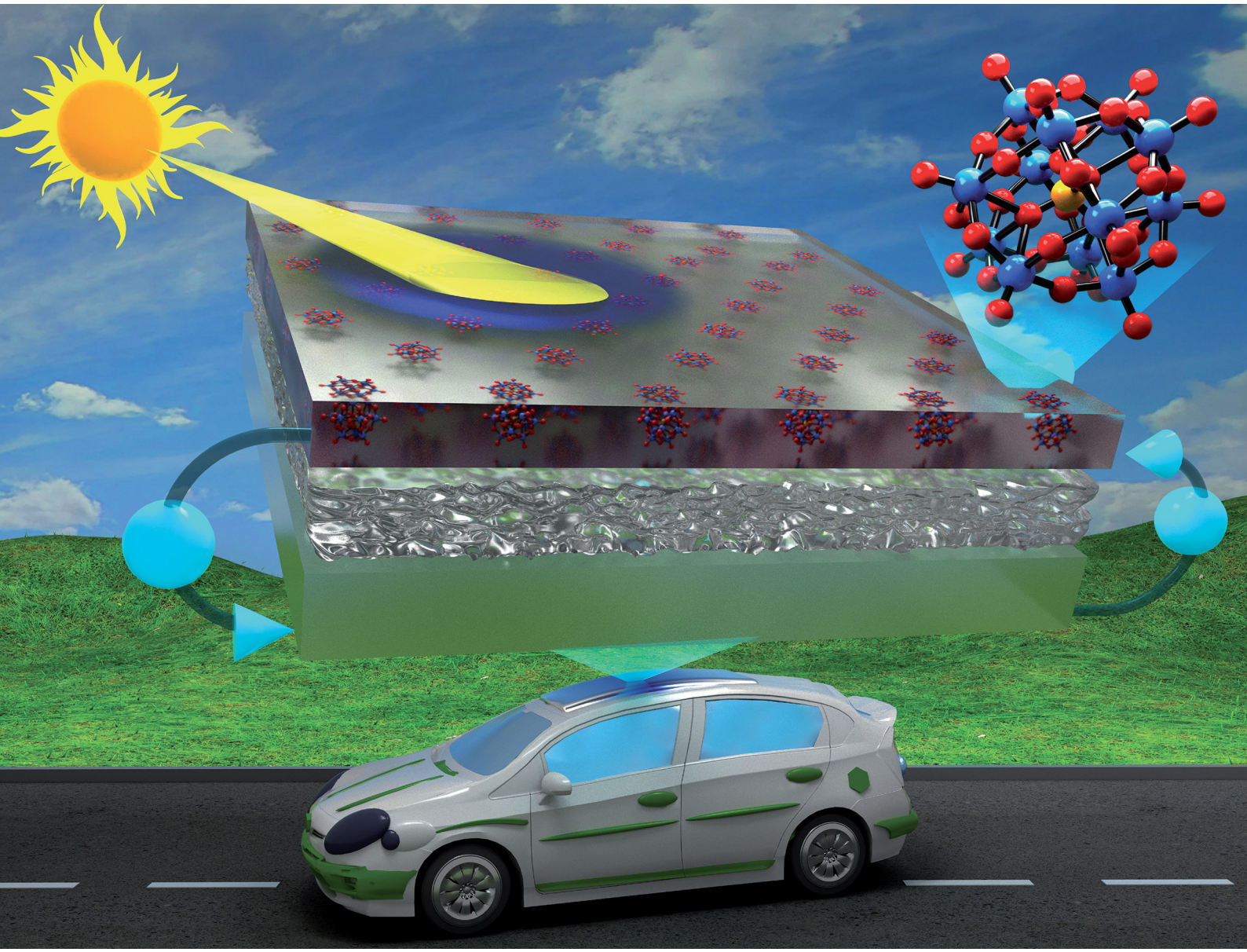

ISSN 1359-7345

ROYAL SOCIETY OF CHEMISTRY

COMMUNICATION

Venkateshkumar Prabhakaran, Grant E. Johnson, Julia Laskin *et al.*
Integrated photoelectrochemical energy storage cells prepared by benchtop ion soft landing

ChemComm

ROYAL SOCIETY OF CHEMISTRY

COMMUNICATION

View Article Online
View Journal | View Issue

Cite this: *Chem. Commun.*, 2022, **58**, 9060

Received 6th May 2022,
Accepted 18th July 2022

DOI: 10.1039/d2cc02595g

rsc.li/chemcomm

Integrated photoelectrochemical energy storage cells prepared by benchtop ion soft landing†

Venkateshkumar Prabhakaran, *[a] Joelle Romo,[a] Ashish Bhattarai,[a] Kyle George,[a] Zachary M. Norberg,[a] David Kalb,[a] Edoardo Aprà, [b] Peter A. Kottke,[c] Andrei G. Fedorov, [c] Patrick Z. El-Khoury, [a] Grant E. Johnson *[a] and Julia Laskin *[d]

The exceptional photochromic and redox properties of polyoxometalate anions, $PW_{12}O_{40}^{3-}$, have been exploited to develop an integrated photoelectrochemical energy storage cell for conversion and storage of solar energy. Elimination of strongly coordinating cations using benchtop ion soft landing leads to a ~370% increase in the maximum power output of the device. Additionally, the photocathode displayed a pronounced color change from clear to blue upon irradiation, which warrants the potential application of the IPES cell in advanced smart windows and photochromic lenses.

Development of efficient energy conversion and storage systems is necessary to meet ever-increasing global energy demands. Solar energy is a renewable and sustainable resource that may be utilized in numerous technologies. In one hour, more energy from the sun reaches the earth than the world population consumes in an entire year.[1] However, the sporadic nature of local solar energy flux necessitates development of efficient energy storage components (*e.g.*, solid-state and redox flow batteries) to achieve a dependable continuous supply of electricity. Many current solar energy harvesting systems, including photovoltaics and solar power concentrators, convert solar energy to electricity.[2,3] These technologies employ energy stored in batteries, fuel cells, and pumped hydroelectric storage, all of which are accompanied by substantial efficiency losses resulting from conversion between different forms of energy. It follows that development of integrated systems that combine solar energy conversion and storage in a single photoelectrochemical device may be a promising route to improving the efficiency of solar energy utilization.

A photoelectrochemical system that is capable of converting and storing solar energy relies on photo-induced reactions of redox-active species.[4–6] To date, several types of integrated photoelectrochemical storage systems have been explored.[7–10] Notable approaches include the use of a photosensitizer on one side of an electrode with a redox couple on the other side connected through a redox mediator (*e.g.*, dye-sensitized solar cells). Existing methods require at least two chemical moieties, one for trapping photons to produce electron–hole pairs and another for transferring electrons to redox molecules for storage. This paradigm suffers from inefficiencies during transmission of electrons from one moiety to another, lower conductivity of photosensitizers, and duty cycle performance issues.[11,12] Therefore, combining both solar energy conversion and storage together using a single bifunctional moiety may boost the utilization of such integrated technologies.

Polyoxometalates (POMs) are a class of metal-oxides that are of interest to energy technologies due to their exceptional multi-electron redox activity and stability.[13–15] Previous studies also demonstrated the photo- and electro-chromic properties of POMs (*i.e.*, their color change from clear to blue upon reduction).[16–18] The photochromic properties of POMs during solar harvesting/energy storage processes have potential applications where standalone power needs are necessary, for example in "smart" windows and lenses. Traditionally, smart window and photochromic lens technologies use hydrogels or metal oxide layers which darken in sunlight, thereby providing shade and cooling.[19–21]

Herein, we demonstrate the working principle of a novel integrated photoelectrochemical energy storage (IPES) cell composed of a photocathode coated with $PW_{12}O_{40}^{3-}$ (WPOM), an anode containing a counter redox couple, and an ionically conductive membrane separating the two electrodes. In the cell, a photo-induced redox conversion of WPOM at the indium tin oxide (ITO) cathode is countered by a redox reaction at the anode, which produces an electrochemical potential difference that drives electrons between the electrodes. Ferrocenemethanol was

[a] *Physical Sciences Division, Pacific Northwest National Laboratory, Richland, WA, 99352, USA. E-mail: venky@pnnl.gov, Grant.Johnson@pnnl.gov*
[b] *Environmental Molecular Sciences Laboratory, Pacific Northwest National Laboratory, Richland, WA, 99352, USA*
[c] *School of Mechanical Engineering, Georgia Institute of Technology, Atlanta, GA, 30332, USA*
[d] *Department of Chemistry, Purdue University, West Lafayette, IN, 47907, USA. E-mail: jlaskin@purdue.edu*

† Electronic supplementary information (ESI) available. See DOI: https://doi.org/10.1039/d2cc02595g

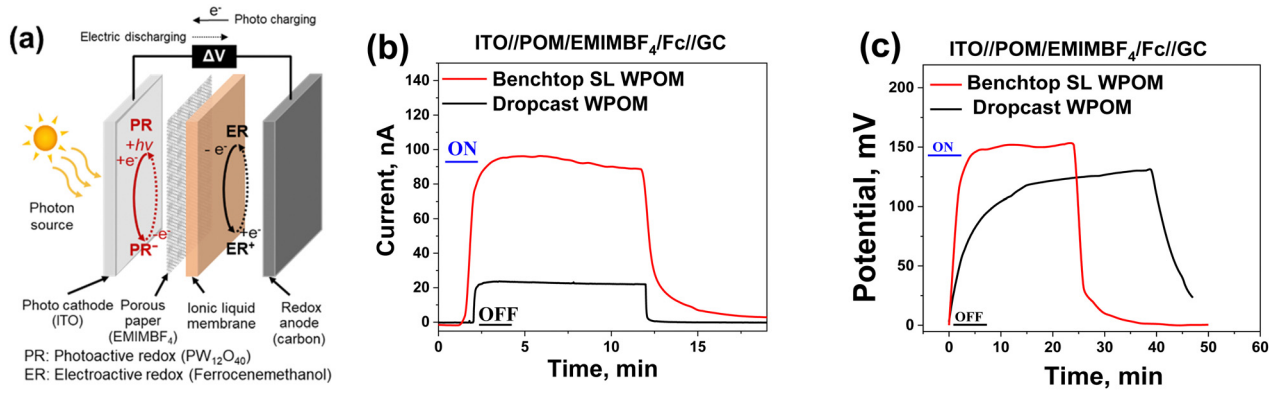

Fig. 1 (a) Schematic diagram of the integrated photoelectrochemical energy storage (IPES) cell in which light absorbed by WPOM at the ITO photocathode is converted into electrical current through the photoredox activity of WPOM at the cathode; counter redox activity of Ferrocenemethanol at the carbon anode serves as a source of electrons in the system. Photocharge discharge profiles of IPES cells with drop cast and benchtop SL WPOM on ITO cathodes and GC as the counter anode. (b) current response, (c) potential response. Approximately $\sim 10^{15}$ WPOM ions were deposited onto ITO in each experiment.

selected as the counter redox couple at the carbon anode and acts as energy storage component of the IPES cell during photocharging of WPOM.[22–24] A solid ionic liquid membrane separates the electrodes and ensures ionic transport throughout the cell. A schematic diagram of the IPES cell is shown in Fig. 1a. To enable a meaningful comparison, POMs were deposited onto the ITO photocathode using both conventional solution-based drop casting and benchtop ion soft landing (SL), a versatile and highly-controlled approach for the modification of interfaces that efficiently removes neutral solvent molecules and counter ions.[25–31] SL of mass- and charge-selected POM anions in vacuum was shown to enhance the redox activity and stability of POMs at electrochemical interfaces due to more intimate contact between discrete individual POMs and the electrode and elimination of larger less active aggregates that form in the presence of counter-ions and solvent. The drop cast cathode, in comparison, contains both POM anions and strongly-coordinating counter cations (*e.g.*, Na^+), which have been shown previously to reduce the redox activity of POMs.[25,27,30]

Initially, the intrinsic electrochemical activity of WPOM and ferrocenemethanol on ITO and glassy carbon (GC), respectively, was evaluated by cyclic voltammetry (CV) (Fig. S1, ESI†). We found that a potential difference of $\sim$200 mV may be achieved when WPOM is used in the IPES on the photocathode and ferrocenemethanol on the redox anode. The 1-ethyl-3-methylimidazolium tetrafluoroborate ($EMIMBF_4$) ionic liquid used as an electrolyte during the electrochemical measurements in the IPES cell provides an expanded potential window for WPOM compared to an aqueous electrolyte. The IPES cells were fabricated using the procedure described in the experimental section of the ESI.† The solar energy conversion and storage in the as-prepared IPES cells were evaluated by measuring the photocurrent and potential that develop across the cells with and without simulated solar irradiation [125 W m^{-2} Ultraviolet-visible (UV-vis) light source]. The current and potential measurements were performed separately using the same type of IPES cell. When the cell was charged (irradiation ON), reduction of WPOM at the photocathode occured simultaneously with oxidation of ferrocenemethanol at the anode. The reverse reactions take place during discharge (irradiation OFF) of the IPES cell. The photo-reduction and counter oxidation reactions produce the photocurrent and potential difference across the cell. To assess the effect of electrode surface morphology on the kinetics of the ferrocenemethanol redox reaction and overall IPES cell performance, several types of anodes such as planar (GC, gold and ITO) and porous carbon nanotube (CNT) types were examined using the same drop cast photocathodes. We found that the cell performance of carbon-based cathodes was the highest (Fig. S2, ESI†) and stable for at least 3 cycles (Fig. S3, ESI†). Therefore, carbon-based counter electrodes were used for all further experiments. Furthermore, characterization of the cathode with *in situ* UV-vis spectroscopy confirmed the expected color change of WPOM during the redox transition under solar irradiation (Fig. S4 and S5, ESI†).

The effect of counter ions on the activity of the photocathodes was evaluated by comparing cathodes prepared by drop casting and benchtop SL. The photocharge–discharge profiles of the two types of cathode with GC as the counter anode are shown in Fig. 1(b and c). The photocurrent of the soft landed cells attained a maximum of 98 nA with a potential of 150 mV (1.47×10^{-8} W) which is $\sim$370% higher power than the drop cast cells with a maximum current of 25 nA with a potential of 125 mV (3.13×10^{-9} W). Therefore, elimination of inactive Na^+ counter cations and solvent using benchtop SL substantially improved the photo-induced redox activity of WPOM at the photocathode of the IPES cell. Furthermore, both the drop cast and soft landed cells showed rapid current response upon initial irradiation when the light source was first turned ON (Fig. 1b). In contrast, a substantially slower response in the cell potential during the charge–discharge process was observed for the drop cast cell (Fig. 1c). Specifically, the drop cast cell reached its maximum potential in $\sim$40 min while the cell prepared using benchtop SL reached its maximum potential in less than 5 min, which is an 8× improvement in temporal response. A similar trend in current

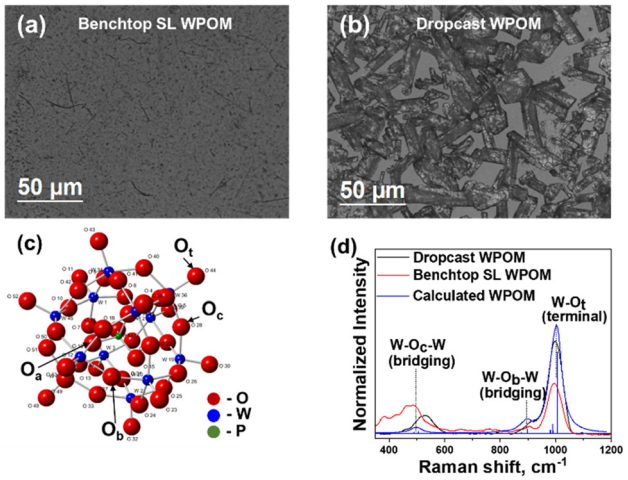

Fig. 2 Optical micrographs of (a) benchtop SL and (b) drop cast WPOM on ITO, (c) calculated structure of $PW_{12}O_{40}^{3-}$ at the B3LYP/def2TZVP level of theory and (d) experimental and calculated Raman spectra of solution drop cast and benchtop SL WPOM on ITO. Approximately $\sim 10^{15}$ WPOM ions were deposited onto ITO in each case.

was observed during the discharge process. The enhanced performance of soft landed photocathodes in both current and potential response to switching on and off of the irradiation was consistent throughout multiple experiments. These results demonstrate a substantial improvement in the temporal current and potential response of the IPES due to the facile photoinduced kinetics occurring at the soft landed photocathode.

Further understanding of the effect of counter cations on the spatial distribution of active WPOM on ITO at the macroscopic level was obtained using optical microscopy and hyperspectral optical absorption microscopy. The optical micrographs of benchtop SL and drop cast WPOM on ITO are shown in Fig. 2a and b, respectively. Visible aggregates of WPOM ~10–15 μm in size are observed on the drop cast cathode at both higher and lower magnification, whereas the soft landed cathode exhibits uniform features all over the imaged region. Hyperspectral optical absorption microscopy provides insight into the spatial distribution of absorption signatures at selected wavelengths (*e.g.*, ~ 500 nm as shown in Fig. S6, ESI†) that correspond to known electronic transitions in WPOMs. The profiles obtained across a 250 μm line on both the soft landed and drop cast WPOM on ITO using 500 nm light with a spatial resolution of 435 nm (spectral resolution: 4.7 nm) are shown in Fig. S6 (ESI†). The consistently narrow absorbance peaks observed across the sampled region of soft landed WPOM on ITO cathodes indicate a more uniform distribution of WPOM produced by benchtop SL, whereas the larger variations of absorbance in the line profile of drop cast WPOM provides evidence of WPOM aggregation due to the presence of coordinating counter ions and solvent. This result is consistent with our previous transmission electron microscopy (TEM) observation of aggregate formation due to the presence of counter cations alongside POM on CNT electrodes.[25,27,30]

The effect of counter cations at the photocathode on the chemical state of WPOM on ITO was examined using Raman micro-spectroscopy. The experimental spectra of drop cast and soft landed WPOM on ITO, along with the theoretically calculated Raman spectrum of gas-phase $PW_{12}O_{40}^{3-}$, are shown in Fig. 2d. Based on our molecular simulations, the Raman peaks at 1000, 895, and 490 cm^{-1} observed for soft landed WPOM are assigned to the normal modes involving the terminal (W = O_t) and bridging (W–O_b–W and W–O_c–W) bands, respectively.[32,33] The experimental spectrum obtained for the soft landed WPOM on ITO is in good agreement with the theoretically calculated Raman spectrum of the gas-phase $PW_{12}O_{40}^{3-}$. For the drop cast $Na_3PW_{12}O_{40}$ on ITO, the Raman peaks observed at 1000 and 895 cm^{-1} are in reasonable agreement with the calculated positions of the W = O_t and W–O_b–W bands, respectively. However, the peak involving the W–O_c–W mode is substantially blue-shifted by 45 cm^{-1} appearing at 535 cm^{-1}. This observation is consistent with prior reports in which counter ions were found to substantially shift the wavenumbers of the normal modes of moieties at coordination sites.[32] We thus attribute the blue shift of the W–O_c–W Raman band to the presence of strongly coordinating cations around $PW_{12}O_{40}$ in the drop cast sample. The counterions, in turn, may lead to the formation of larger POM aggregates, which impede electron transfer processes and reduce photoredox activity at the electrochemical interface.

In order to optimize the overall performance of the cell, we examined additional factors affecting the redox kinetics of the ferrocenemethanol on the anode. Although the improved redox kinetics of the GC electrode enhance the activity of the redox couple in the IPES cell, the relatively low surface area of the GC electrode may be a factor limiting the overall energy storage and performance of the cell. We hypothesized that a porous carbon electrode may improve the total current/voltage output of the cell by allowing a larger amount of ferrocenemethanol molecules to participate in the redox counter reaction at the anode. To test this premise, we used CNT-coated carbon paper with higher surface porosity (pore diameter ~ 2 μm) as a redox anode. The current and potential responses of IPES cells fabricated with CNT paper as the anode and photocathodes prepared using either drop casting or benchtop SL of WPOM onto ITO are shown in Fig. S7 (ESI†). For the drop cast cell, a maximum current of 400 nA with a potential of 370 mV was achieved which is substantially higher than for all of the other drop cast cells discussed so far. This observation confirms our hypothesis that the overall cell performance may be improved by an increased number of ferrocenemethanol molecules participating in the redox reaction at the anode. On the other hand, the soft landed IPES with CNT counter electrode showed a further significant increase in the cell performance with a maximum current of 1500 nA with a potential of ~550 mV. These results indicate a ~4x increase compared to the drop cast electrode. The response time of the soft landed IPES cell to attain steady state current and potential is relatively longer than the drop cast electrode which may be attributed to a diffusion limitation that exists to counter the large flux of electrons from the highly efficient photocathode reaction.

Overall, the results presented herein demonstrate a novel IPES cell, which enables harvesting, conversion, and storage of solar energy in a single device. The cell exploits the exceptional

photo- and electro-chromic properties of WPOM to substantially enhance the performance of the photocathode. Several key factors that affect the performance of the IPES cells were explored including the surface properties of the photocathodes, presence of coordinating counter ions, spatial distribution of WPOM, and the type of anode. The effect of counter cations was examined using benchtop SL, which enables deposition of POM anions in the absence of cations and solvent. The performance of the IPES cells was increased by ~370% by eliminating countercations and solvent molecules at the photoredox cathode. Micro- and spectroscopic analysis of the drop cast electrodes reveals that both aggregation and the presence of strongly coordinating cations around WPOM on the electrodes are detrimental to performance. In contrast, both Raman spectroscopy and hyperspectral microscopy indicate that photocathodes prepared using benchtop SL contain more uniformly distributed WPOM, which substantially improve the electrochemical performance of the photocathode. In summary, better fundamental understanding of the redox mechanism of photochromic materials and associated electron transfer processes in a single interface will enable the rational design of integrated photoelectrochemical energy conversion and storage technologies.

V. P., J. R., K. G., Z. M. N., D. K., G. E. J., and J. L. acknowledge support from the US Department of Energy (DOE), Office of Science, Office of Basic Energy Sciences (BES), Chemical Sciences, Geosciences and Biosciences (CSGB) Division. VP and PZE acknowledge support from the Laboratory Directed Research and Development Program at Pacific Northwest National Laboratory (PNNL). J. R., K. G., and Z. M. N. worked as undergraduate interns at PNNL supported by the DOE's Science Undergraduate Laboratory Internship Program (SULI). EA acknowledges support from the Center for Scalable Predictive methods for Excitations and Correlated phenomena (SPEC), which is funded by the U.S. DOE, Office of Science, BES, CSGB Division as part of the Computational Chemical Sciences (CCS) program at the PNNL. P. A. K. was supported by the National Institute of General Medical Sciences of the National Institutes of Health under Award Number R01GM112662 (DRILL design and simulations). A. G. F. was supported by the US DOE, Office of Science, BES, under Award #DE-SC0010729 (electrospray-based nanomaterial deposition). This research also benefited from resources provided by PNNL Institutional Computing (PIC). The research was performed using EMSL, a national scientific user facility sponsored by the DOE's Office of Biological and Environmental Research and located at PNNL. PNNL is operated by Battelle for DOE under Contract DE-AC05-76RL01830.

Conflicts of interest

There are no conflicts to declare.

Notes and references

1 J. Tsao, N. Lewis and G. Crabtree, *Solar FAQs*, US Department of Energy, 2006, 1–24.
2 S. R. Kurtz, Opportunities and challenges for development of a mature concentrating photovoltaic power industry, *National Renewable Energy Laboratory*, 2012, DOI: 10.2172/935595.
3 M. H. Shubbak, *Renewable Sustainable Energy Rev.*, 2019, **115**, 109383.
4 Z. Wei, D. Liu, C. Hsu and F. Liu, *Electrochem. Commun.*, 2014, **45**, 79–82.
5 P. Liu, Y. L. Cao, G. R. Li, X. P. Gao, X. P. Ai and H. X. Yang, *ChemSusChem*, 2013, **6**, 802–806.
6 G. Cai, J. Wang and P. S. Lee, *Acc. Chem. Res.*, 2016, **49**, 1469–1476.
7 Q. Yang, Q. Hao, J. Lei and H. Ju, *Anal. Chem.*, 2018, **90**, 3703–3707.
8 J. Azevedo, T. Seipp, J. Burfeind, C. Sousa, A. Bentien, J. P. Araújo and A. Mendes, *Nano Energy*, 2016, **22**, 396–405.
9 X. Xia, J. Luo, Z. Zeng, C. Guan, Y. Zhang, J. Tu, H. Zhang and H. J. Fan, *Sci. Rep.*, 2012, **2**, 981.
10 G. Hodes, J. Manassen and D. Cahen, *Nature*, 1976, **261**, 403–404.
11 Q. Li, Y. Liu, S. Guo and H. Zhou, *Nano Today*, 2017, **16**, 46–60.
12 M. Yu, W. D. McCulloch, D. R. Beauchamp, Z. Huang, X. Ren and Y. Wu, *J. Am. Chem. Soc.*, 2015, **137**, 8332–8335.
13 G. Zhang, Z. Chen, T. He, H. Ke, Y. Ma, K. Shao, W. Yang and J. Yao, *J. Phys. Chem. B*, 2004, **108**, 6944–6948.
14 C. L. Hill, *Chem. Rev.*, 1998, **98**, 1–2.
15 J. Song, Z. Luo, H. Zhu, Z. Huang, T. Lian, A. L. Kaledin, D. G. Musaev, S. Lense, K. I. Hardcastle and C. L. Hill, *Inorg. Chim. Acta*, 2010, **363**, 4381–4386.
16 P. Gómez-Romero and N. Casañ-Pastor, *J. Phys. Chem.*, 1996, **100**, 12448–12454.
17 T. Yamase, *Chem. Rev.*, 1998, **98**, 307–326.
18 H. Ma, J. Peng, Y. Chen, Y. Feng and E. Wang, *J. Solid State Chem.*, 2004, **177**, 3333–3338.
19 Z. Liang, L. Zhao, W. Meng, C. Zhong, S. Wei, B. Dong, Z. Xu, L. Wan and S. Wang, *J. Alloys Compd.*, 2017, **694**, 124–131.
20 S. Kiruthika and G. U. Kulkarni, *Sol. Energy Mater. Sol. Cells*, 2017, **163**, 231–236.
21 X. Cao, N. Wang, J. Y. Law, S. C. Loo, S. Magdassi and Y. Long, *Langmuir*, 2014, **30**, 1710–1715.
22 K. R. Lovelock, A. Ejigu, S. F. Loh, S. Men, P. Licence and D. A. Walsh, *Phys. Chem. Chem. Phys.*, 2011, **13**, 10155–10164.
23 W. Miao, Z. Ding and A. J. Bard, *J. Phys. Chem. B*, 2002, **106**, 1392–1398.
24 L. L. Darren, A. Walsh, B. Mayowa and K. T. Voisey, *Electrochim. Acta*, 2009, **54**, 4647–4654.
25 V. Prabhakaran, B. L. Mehdi, J. J. Ditto, M. H. Engelhard, B. Wang, K. D. Gunaratne, D. C. Johnson, N. D. Browning, G. E. Johnson and J. Laskin, *Nat. Commun.*, 2016, **7**, 11399.
26 V. Prabhakaran, G. E. Johnson, B. Wang and J. Laskin, *Proc. Natl. Acad. Sci. U. S. A.*, 2016, **113**, 13324–13329.
27 G. E. Johnson, V. Prabhakaran, N. D. Browning, B. L. Mehdi, J. Laskin, P. A. Kottke and A. G. Fedorov, *Batteries Supercaps*, 2018, **1**, 97–101.
28 P. Su, V. Prabhakaran, G. E. Johnson and J. Laskin, *Anal. Chem.*, 2018, **90**, 10935–10942.
29 J. Laskin, G. E. Johnson, J. Warneke and V. Prabhakaran, *Angew. Chem., Int. Ed.*, 2018, **57**, 16270–16284.
30 V. Prabhakaran, Z. Lang, A. Clotet, J. M. Poblet, G. E. Johnson and J. Laskin, *ACS Nano*, 2019, **13**, 458–466.
31 G. E. Johnson, D. Gunaratne and J. Laskin, *Mass Spectrom. Rev.*, 2016, **35**, 439–479.
32 E. Grinenval, J. M. Basset and F. Lefebvre, *Inorg. Chem.*, 2010, **49**, 8749–8755.
33 C. M. Teague, X. Li, M. E. Biggin, L. Lee, J. Kim and A. A. Gewirth, *J. Phys. Chem. B*, 2004, **108**, 1974–1985.